

# A high-resolution spectrograph for the 3.6-m Devasthal Optical Telescope of ARIES

Jeewan Chandra Pandey\*, Jayshreekar Pant, Yogesh Chandra Joshi

Aryabhata Research Institute of Observational Sciences. Nainital, India 263001

**Abstract:** A high-resolution spectrograph for the 3.6-m Devasthal Optical Telescope (DOT) of Aryabhata Research Institute of Observational Sciences (ARIES; Nainital, India) is envisaged to achieve the various science goals. The spectrograph will have two modes of spectral resolution (40 000 and 80 000) with a wavelength coverage of 380 - 900 nm. The design of the spectrograph will be similar to many contemporary high-resolution spectrometers in the world and will be based on a modern design using the white pupil concept. It will be a bench mounted fibre-fed spectrograph. In this article, we present the various science goals, technical specifications, and concept of design for the proposed spectrograph.

**Keywords:** Spectrograph – Optical band – high-resolution –echelle

## 1 Introduction

ARIES has recently installed a 3.6-m optical telescope at Devasthal near Nainital (India). This telescope is the most sensitive Indian optical telescope for the study of celestial sources due to its large aperture size and active optics. Briefly, the DOT has a two mirror Ritchey-Chretien optical configuration with a primary diameter of 3.6 m and a secondary diameter of 0.9 m. The effective focal ratio of the telescope is  $f/9$ . The meniscus primary mirror is active and it is supported by pneumatic actuators. It has one axial and two side Cassegrain ports with a science field of view of  $30'$  and  $10'$ , respectively. The operational waveband of the telescope is 350-5000 nm. The DOT has an alt-azimuth mount. The azimuth axes system is equipped with hydrostatic bearings. The tracking accuracy of the DOT is  $< 0.1''$  root-mean-square in open loop for  $\sim 1$  minute and  $< 0.1''$  for about an hour in closed loop mode (Sagar et al. 2012). A detailed description of the 3.6-m DOT can be found in Kumar et al. (2018) and Omar et al. (2017).

Devasthal is located at a longitude of  $79^{\circ}41'04''$  E, latitude of  $29^{\circ}21'40''$  N, and altitude of  $(2424 \pm 4)$  m above mean sea level. The ground level median seeing of the site is  $1.1''$  with a wind speed of  $< 3 \text{ m s}^{-1}$  for 75% of the time. For 35% of the time, the seeing is better than  $1.0''$  (Sagar et al. 2000). The annual variation of the air temperature at the site is  $21.5^{\circ}\text{C}$  to  $-4.5^{\circ}\text{C}$  with a nightly temperature variation of  $\leq 2^{\circ}\text{C}$ . Annually, 80% of the total rain (2 m) falls from June to September. A total of  $\sim 60\%$  and  $\sim 48\%$  nights in a year are found to be spectroscopic and photometric, respectively. The original atmospheric extinction studies at Devasthal resulted in average values of  $k_U = 0.49 \pm 0.09$ ,  $k_B = 0.32 \pm 0.06$ ,  $k_V = 0.21 \pm 0.05$ ,  $k_R = 0.13 \pm 0.04$ , and  $k_I = 0.08 \pm 0.04$  mag (Mohan et al. 1999)

---

\*jeewan@aries.res.in

whereas recent observations by Pandey et al. (2018) show that  $k_U = 0.64 \pm 0.03$ ,  $k_B = 0.39 \pm 0.02$ ,  $k_V = 0.29 \pm 0.02$ ,  $k_R = 0.22 \pm 0.01$ , and  $k_I = 0.17 \pm 0.02$  mag.

Various research activities have been carried out at ARIES in the last few decades using a polarimeter and imager as back-end instruments of meter-class telescopes of ARIES (e.g. Sagar & Joshi, 1983 Pandey & Mahra 1986, Sagar et al. 1999, Durgapal & Pandey 2001, Pandey et al. 2003a, Joshi et al. 2005, Pandey et al. 2005, Joshi et al. 2006, Medhi et al. 2007, Pandey et al. 2009, Joshi et al. 2011, Joshi et al. 2016, Patel et al. 2016, Lata et al. 2016, Joshi & Pandey 2018, etc.). After installation of the DOT, various other front line science programs are initiated using different back-end instruments. The  $4k \times 4k$  CCD imager was the first light instrument for the DOT. Its detailed description is given in Pandey et al. (2018). Few results from this instrument are published in Pandey et al. (2019) and Lata et al. (2019). The TIFR Near-Infrared Imaging Camera-II (TIRCAM2) is another instrument mounted at the DOT. It is a cryo-cooled imaging camera equipped with a Raytheon 512 pixels InSb Aladdin III Quadrant focal plane array sensitive in the 1000 – 5000 nm wavelength band. TIRCAM2 has seven observing filters, namely  $J$  (1200 nm),  $H$  (1650 nm),  $Br\gamma$  (2160 nm),  $K_{\text{cont}}$  (2170 nm),  $K$  (2190 nm), PAH (3280 nm), and  $nbL$  (3590 nm), with field of view of  $86.5'' \times 86.5''$  for the DOT (Baug et al. 2018). A low-dispersion spectrograph-cum-imager has been developed recently at ARIES for the DOT. The instrument is capable of carrying out low-resolution slit spectroscopy in the wavelength range 350 – 1050 nm with a spectral resolution  $< 2000$  along with broad and narrow band imaging. The description of the instrument and its first light observations are mentioned in Omar et al. (2019a, 2019b). The TIFR-ARIES Near Infrared Spectrometer (TANSPEC) is being built for the DOT in collaboration with Mauna Kea InfraRed, LLC (Hawaii, USA). It will be a unique spectrograph which provides a wavelength coverage in the range of 550 – 2540 nm with a spectral resolution of  $\sim 2700$  (Ojha et al. 2018).

The DOT is equipped with both imagers and low-resolution spectrographs in optical and infrared (IR) bands to carry out different science programs. However, there are several science cases which can not be carried out with the DOT equipped with the above-mentioned instruments. Therefore, a high-resolution spectrograph is considered as a major instrument for the DOT. Moreover, the higher the spectral resolution of the spectrograph, the more detailed information about the observed source becomes available to the astronomer. In this article, we give an overview of the various science goals (Section 2), the technical specifications (Section 3), and the concept of the design (Section 4) and its national and international status (Section 5) for the proposed high-resolution spectrograph.

## 2 Science drivers

A brief description of the science program to be carried out with the proposed instrument is mentioned below.

### 2.1 Asteroseismology

In order to fully understand the evolution of stars, detailed information on the processes within the stellar interior is needed. Since the stellar interior is not directly accessible, asteroseismologists use the indirect information contained in stellar oscillations to probe the stellar interiors. There are two families of modes carrying information on different parts of the stellar interior: pressure modes (p-modes; mainly propagating in the envelope) and gravity modes (g-modes; mainly propagating in the core). For a unique asteroseismic modelling, a large number of well-identified modes are needed. Different classes of oscillating stars are found across the Hertzsprung-Russell diagram, which will be studied using the proposed spectrograph. The  $\beta$  Cephei and  $\delta$  Scuti stars (pulsating in low order p- and g-modes with periods of the order of hours) and the slowly pulsating B and  $\gamma$  Doradus stars

(pulsating in high order g-modes with periods of the order of days) are situated along the upper part of the main sequence. Asteroseismology of p-modes in Sun like stars may help to test detailed models of stellar structure and evolution (e.g. De Mauro 2016, Joshi & Joshi 2015). Using the proposed high-resolution spectrograph, we would like to study the line-profile variations in these pulsating stars to detect and identify the various modes of oscillation.

## **2.2 Doppler tomography of the stellar surface**

Doppler tomography is an inversion technique to produce images of surface features on stars using a series of high-resolution spectral line profiles (Rice 2002, Collier-Cameron et al. 2001). The principle of Doppler imaging is fairly well known (Vogt & Penrod, 1983) but the number of applications has grown over last two decades thanks to the higher sensitivity of spectrographs and the modern methods of computation. This has made Doppler tomography one of the most reliable tools to estimate the spatial distribution of the temperature and chemical abundances over the stellar surface. It requires high-resolution spectra ( $R > 60\,000$ ) with a signal-to-noise ratio (SNR) of  $\sim 200$  and a good phase coverage. There are many exciting results from this technique. For example, Doppler images for both stellar components of a binary star  $\sigma^2$  CrB showed evidence for the coexistence of cool and warm spots on both stars (Strassmeier & Rice 2003). The Doppler imaging technique can be also applied to other stars like chemically peculiar magnetic stars, cataclysmic variables, etc. With the proposed high-resolution spectrograph, we would be able to carry out very comprehensive studies of these stars. Such investigations are important to understand the nature and origin of various activities in them.

## **2.3 Abundance studies**

The study of the surface stellar composition is important because, in several instances, the surface composition reflects internal nucleosynthesis and mixing, and thus offers a way to probe the internal stellar processes. These studies involve the predictions of surface abundances through nucleosynthesis and mixing models computed in the framework of stellar evolution models, the recording of stellar spectra through a high-resolution spectrometer, the computation of stellar atmosphere models (possibly in three dimensions) matching the properties of the considered star, and their analysis through radiative-transfer codes (e.g. Kurucz 2014). Oxygen abundances are derived from the high-excitation OI triplet. The central wavelengths of the line of the OI triplet are at 777.2 nm, 777.42 nm, and 777.5 nm. With a low/medium-resolution spectrum, this triplet is blended. Therefore, a high-resolution spectrum is ideally suited to do abundance studies.

## **2.4 Spectroscopy and ground-based follow-up of exoplanets**

Since the first discovery of a planet around a normal star (51 Peg: Mayor & Queloz 1995), more than 4000 exoplanets have been discovered and exoplanet research has become an established and cutting-edge branch of astronomy and planetary sciences. In fact, the astronomers' attention is no longer restricted to the discovery of the exoplanets but has progressively widened to their characterization. A planetary atmosphere contains valuable information on the formation and evolution of the planet. Transit spectroscopy has been demonstrated to be a powerful tool for the characterization of planetary atmospheres (e.g. Sing et al. 2016). The wavelength-dependent absorption during the transit is indicative of the composition of its atmosphere such as gases, hazes, and clouds. High-dispersion spectroscopy on a large telescope such as the DOT can overcome the difficulty to get high SNR observations inherent to the many orders of magnitude that separate the brightness of a planet and that of its stellar host. In addition to the characterization, the ground-based radial velocity (RV)

follow-up for the TESS mission (Ricker et al. 2014) will be essential to confirm any candidates open to the community. By adding an appropriate gas absorption cell wavelength calibrator, the proposed instrument can contribute to the confirmation and characterization of the TESS planet candidates. Those newly discovered targets will be also important for the Thirty Meter Telescope (TMT) project to which the Indian community will contribute.

## **2.5 Peculiar eruptive young stellar objects**

The standard model for star formation suggests a constant accretion rate (e.g. Shu et al. 1987). However, few past studies based of low-mass star forming regions (Dunham et al. 2010) showed that the luminosities of young stellar objects are systematically low compared to the standard model (Dunham et al. 2010). In addition to this, the discovery of Very Low Luminosity Objects (VeLLOs; Young et al. 2004) and their associated strong outflows (Andre et al. 1999) raised questions about the steady accretion process. As a result, an alternate mechanism termed the episodic accretion process has been suggested to account for these observational phenomena (Lee et al. 2007). The episodic accretion process is characterized by two phases: burst and quiescent accretion. FU Orionis-type objects (FUors) have been proposed as prominent examples of burst accreting protostars, while VeLLOs have been proposed as objects in the quiescent phase of the episodic accretion process. This episodic accretion process is the most promising candidate to explain many open problems in star formation like the luminosity problem, discontinuity in outflows etc. During an outburst, the accretion rate increases by a factor of 10 to 100. As a consequence of the eruptive accretion, these protostars exhibit large winds and outflows (Croswell et al. 1987), which are inferred from P Cygni profiles of  $H\alpha$  and other lines. The spectral characteristics of FUors are broad blue-shifted emission lines, IR excess, and near-IR CO overtone features that are consequences of the energetic burst of accretion-driven viscous heating of the disk. Based on these characteristics, Hartmann & Kenyon (1996) and Reipurth & Aspin (2010) identified about a dozen FUors, although in many cases the initial outburst had not been observed. Very little pre-outburst data exists for FUors: few have been studied from the pre-burst phase to the burst phase and a pre-outburst optical spectrum is observed in rare cases (e.g. V1057 Cyg; Kopatskaya et al. 2013). High-resolution spectra ( $R > 50\,000$ ) covering the two KI lines near 770 nm and the CaII triplet lines near 850 nm can be used to detect P Cygni profiles in the KI,  $H\alpha$ , and CaII lines and can trace the disk component as well as the outflow. Monitoring the variation of spectral features will help our understanding of the kinematic structures and of their temporal variations of these sources in its pre-outburst state.

## **2.6 Study of multiple stellar populations in galactic globular clusters**

The longstanding notion that galactic globular clusters (GCs) are simple stellar populations is now challenged by the discovery of multiple populations (MPs) in an increasing number of GCs in the Milky Way (Gratton et al. 2012). Photometry is a time efficient way of revealing MPs, but high-resolution spectroscopy allows a deeper insight into GC formation and internal stellar evolution by providing elemental abundances for a number of elements with a variety in nucleosynthetic origin. Various studies have shown that all galactic GCs have at least a spread (or anti-correlation) in the content of their light elements O and Na. In some cases, a spread in Mg and Al is also observed (e.g. D'Ercole et al. 2010). This spread is due to the early evolution of each cluster that is initially formed by the first generation of stars that have the same chemical composition of field stars at the same metallicity. The subsequent generations of stars (Na-richer and O-poorer) are formed from gas polluted by ejecta of evolved stars of the older generation (Na-poorer and O-richer). This is the so-called multiple population phenomenon. Basic requirements for this program are a spectral range of

400 – 700 nm, a spectral resolution of  $\sim 40\,000$ , and a SNR  $> 50$  at 600 nm for stars with a visual magnitude between 11 and 15 mag.

## **2.7 Measurements of ${}^6\text{Li}/{}^7\text{Li}$ in metal poor halo stars**

A long-standing effort in astrophysics has involved searches for signatures of unstable particles that might have existed in the early universe, but have long since become extinct. The precision that exists in the abundances of the nuclides produced in big bang nucleosynthesis (BBN) suggests that primordial nucleosynthesis is a good place to look for such signatures. In that context, it is of considerable interest that recent observations of metal-poor halo stars indicate that the primordial abundances of both  ${}^6\text{Li}$  and  ${}^7\text{Li}$  may not be in agreement with the predictions of standard BBN. Specifically, the  ${}^6\text{Li}$  appears to have an abundance plateau similar to that for  ${}^7\text{Li}$  in very low metallicity stars (e.g. Charbonnel & Primas 2005). This suggests a primordial abundance. However, the abundance value is roughly a factor of 1000 larger than predicted in standard BBN (e.g. Asplund et al. 2006). To observe  ${}^6\text{Li}$  and  ${}^7\text{Li}$  from metal poor stars, we need a high-resolution spectrograph ( $R \sim 80\,000$ ) on a 4-m class telescope like the DOT.

## **2.8 Supernovae**

Supernovae (SNe) studies with several science goals are being carried out since the last few decades by using the imager and low-resolution spectrograph at ARIES (e.g. Singh et al. 2018, Misra et al. 2008, Pandey et al. 2003b). The following additional science goals will be addressed with the proposed high-resolution spectrograph.

The estimation of the total extinction (galactic and host) is important in supernovae studies to calculate the absolute magnitudes and the total bolometric luminosity. The host extinction is estimated using the equivalent width of the NaI-doublet resulting from the host interstellar matter. In many cases, this NaI-doublet is not seen if the host extinction is very small or the spectra are of low resolution. A high-resolution spectrum is required to clearly see the two NaI components due to the Milky Way and the host in order to estimate the extinction.

Asymmetric profiles of oxygen and calcium have sawtooth profiles when seen through high-resolution spectroscopy. After smoothing the spectra with a boxcar, one can see the actual clumpiness of the ejecta. Thus, the scale of clumps is basically hidden by the resolution of the observations. A high-resolution spectrum of such a profile will allow us to estimate the velocity of the clumps and enable a detailed study of the clumpiness of the ejecta.

The uncertainty of the edges of the lines at zero intensity as well as a large number of overlapping lines makes the interpretation of measured velocities problematic. This is also related to the line blending that is often seen in low-resolution spectra.

The nitrogen left in the helium envelope from the CNO burning gives strong NII emission lines at 654.8 nm and 658.3 nm that dominate over  $\text{H}\alpha$  absorption. The hydrogen envelopes of type IIb SNe are too small and diluted to produce any noticeable  $\text{H}\alpha$  emission or absorption after 150 days, so the nebular phase emission seen around 655 nm is most likely caused by NII. High-resolution spectroscopy will therefore help to understand the nebular phases of SNe evolution.

## **3 Proposed technical specifications**

For the above mentioned scientific programs, we require the following technical specifications:

1. Looking into the general research interest of Indian Astronomical community, we concluded that there is a need for two spectral resolution modes on the ARIES high-resolution spectrograph. The lower resolution should cover most of the general science requirements while the higher resolution should be different from those of other high-resolution spectrographs that already exist in India (typically  $\sim 60\,000$ ; see Section 5). Therefore, two modes of the spectral resolution of 40 000 and 80 000 are favoured for the new spectrograph.
2. The instrument needs to yield a complete wavelength coverage in the optical domain from 380 nm to 900 nm in a single exposure.
3. The spectrograph should be able to record simultaneously the spectrum of an object and/or sky. Alternatively, it will have the possibility to interleave the object spectrum and a wavelength calibration spectrum. The instrument should also be able to record at the same time the spectrum of the faint object along with that of the adjacent sky.
4. The total throughput depends on the individual efficiency of the telescope, spectrograph, detector, optical fibre etc. A peak throughput between 15 – 20% is necessary to get good SNR spectra of stars up to 12-15 mag. At the lower resolution and a reduced SNR, a faint limit of 15 mag may be reached. This high throughput can be obtained by using the very efficient dual pupil design of Baranne (1988).
5. The different science programs each need a specific RV stability. There are certain programs needing a RV stability as low as 2 – 3  $\text{m s}^{-1}$ . This stability can be achieved by obtaining simultaneous calibration spectra (Th-Ar or iodine cell). Moreover, a high mechanical precision, a high stability of the optical components, and controlled thermal and pressure environments are mandatory.
6. The stray light should be below 2% of the signal within the orders for flat-field observations.
7. Fully automated focusing, observing, and calibration functions are requirements of the instrument.
8. The instrument should work under the environmental conditions as mentioned in Section 1.

## 4 Proposed optical design

The instrument will consist of three units, namely a spectrograph unit, an interface plus calibration unit, and a detector. The spectrograph is aimed to provide a high throughput and a robust operation. It will be a fibre fed spectrograph where an optical fibre from the telescope focal plane would carry the light towards the spectrograph. The design of the spectrograph will be based on the white pupil concept (Baranne 1988). In the design, a fibre with a diameter of 100  $\mu\text{m}$  will be used to cover 1.5'' aperture of the sky. An image slicer will be used to slice the image of the fibre exit into two halves to reduce the effective slit width and to double the spectral resolution. An off-axis parabolic mirror (main collimator) will be used for collimation of the spectrograph beam. The collimated beam is diffracted by the echelle grating and collected again by the main collimator. The diameter of the collimator beam is  $\sim 161$  mm. The echelle grating with a groove spacing of 52.6  $\text{gr mm}^{-1}$  and blazed angle of 69.7° will be slightly rotated out of the dispersion plane to separate the incident beam from the diffracted beam. The diffracted beam then will go to the flat folding mirror in the vicinity of the intermediate focal plane. After that, the dispersed beam will be again collimated by the transfer

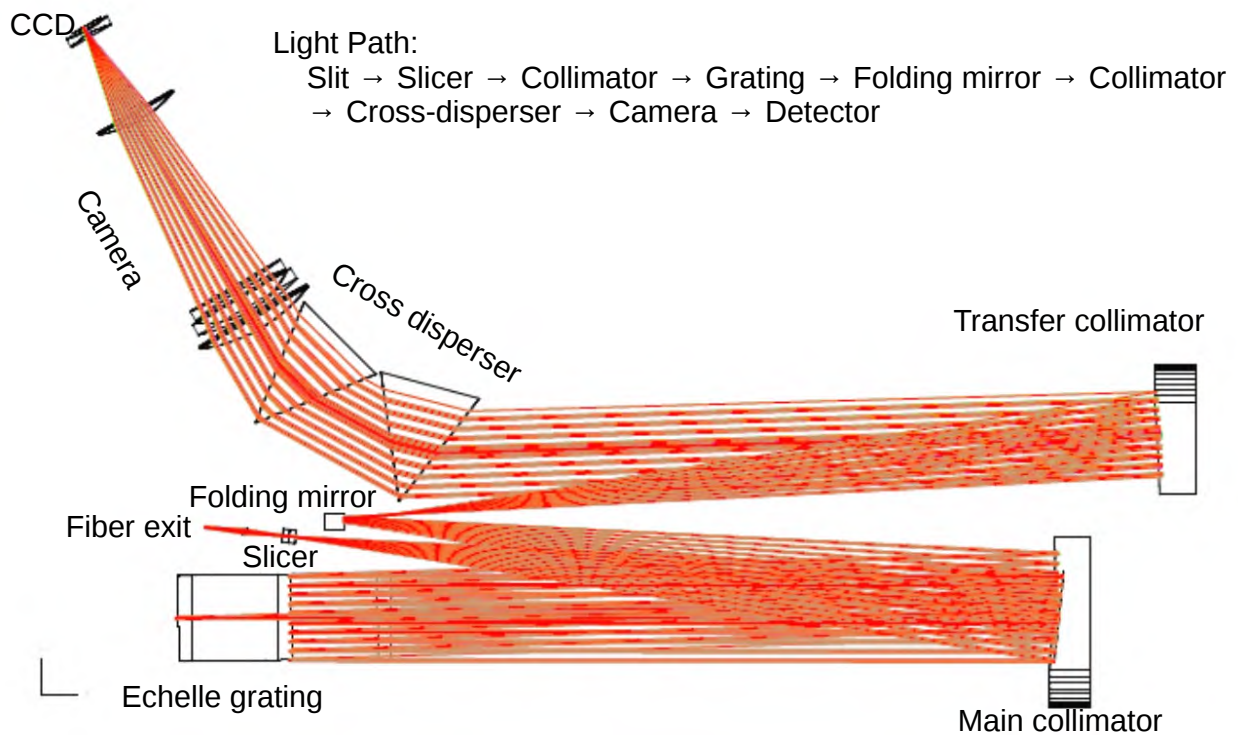


Figure 1: Optical layout of the spectrograph.

collimator and directed towards the cross-disperser prisms. The white pupil will be formed between the cross-disperser and the camera. Finally, the camera will focus the spectrum on the detector. The schematic of the spectrograph design is shown in Fig. 1.

The spectrograph will be mounted on an optical bench inside the telescope pier of the DOT in the controlled environment. The telescope interface plus calibration unit will be mounted in one of the side ports of the telescope. It connects the spectrograph mounted in the isolated environment with the telescope through an optical fibre. The optical layout of this unit is shown in Fig. 2. An atmospheric dispersion corrector (ADC) wheel will be located in front of the telescope focus and the  $f/9$  beam of the telescope passes through the ADC prisms to correct the atmospheric dispersion effect. A guiding unit will be used for centring the stellar image in the fibre. The guiding unit images the telescope focal plane, or more precisely, the fibre location onto the guiding detector. A pierced concave mirror will be used at the telescope focal plane. It will have two holes corresponding to the fibre locations of the object and sky/calibration. This mirror will be slightly tilted ( $\sim 8^\circ$ ) so that it reflects the image of the observed field to an off-axis folding mirror which directs the beam to the guiding optics. The guiding optics images the telescope focal plane, located on the concave mirror, on the guiding detector. The telescope interface unit also consists of the calibration light projection (CLP) optics. The CLP system will inject light coming from the calibration unit into the fibres located at telescope focal plane. This system consists of two lenses and one mirror. The first lens will collimate the beam exiting from the calibration unit whereas the second lens will focus the calibration light on to the fibre situated at telescope focal plane with the help of an on-axis folding mirror. At least two calibration light sources are required for calibrating the spectrograph. The continuum lamp (also called flat-field lamp) will provide a continuum spectrum over the 380 – 900 nm wavelength range of the spectrograph and a hollow-cathode thorium-argon (Th-Ar) lamp forms the basis for the wavelength calibration.

Optical fibres will be used to guide the light coming from the telescope focal plane to the spectrograph, which is mounted on the optical bench in the controlled environment. Two optical fibres at

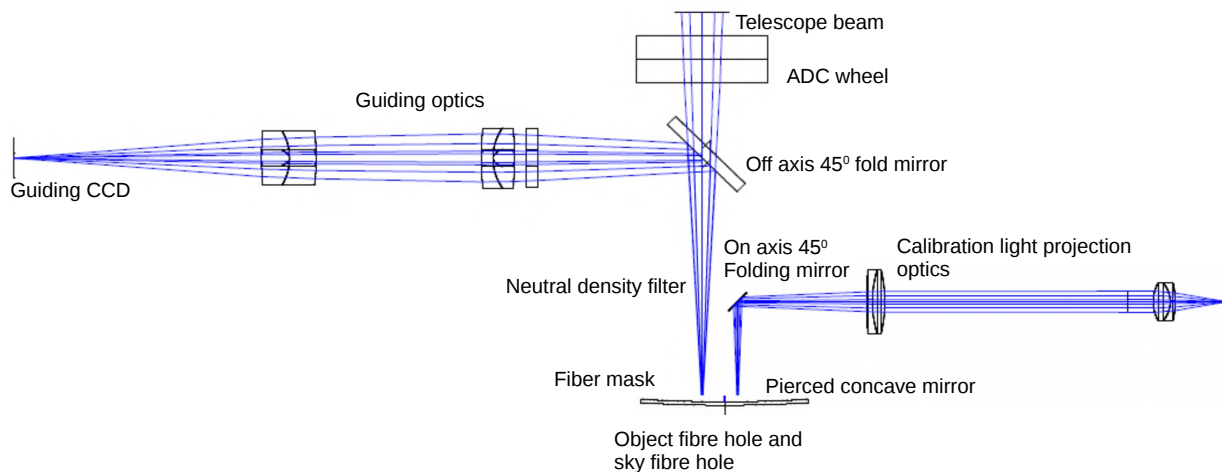


Figure 2: Optical layout of the telescope interface plus calibration unit.

the telescope focal plane will be used. One fibre will capture the star's light for producing the science spectrum whereas the other fibre will be used to image the sky or calibration light. The additional advantage of using optical fibres is that it provides mechanical isolation for the instrument. Also mounting the instrument away from the telescope gives the luxury of keeping the instrument in a precisely controlled environment avoiding the effects of temperature, atmospheric pressure, and relative humidity. So, in a nutshell, optical fibres provide a clear cut advantage in terms of instrument stability. But the introduction of optical fibres causes transmission losses and requires additional optics to inject the light efficiently into the fibre. The  $f/9$  telescope beam will be converted to a  $f/3.6$  beam suitable for optical fibres using a microlens which will be glued on top of the fibre entrance. The telescope pupil will be reimaged at the fibre entrance using this microlens. The focal ratio adaptation optics will be used to slow down the  $f$ -ratio of the beam to be accepted by the spectrograph.

Fig. 3 shows the shape of the echellogram with the location of the start, the center, and the end of a few orders. A total of 55 spectral orders from order 40 to order 94 will be imaged on the detector. Only the free spectral range of each order is shown, while in reality, the orders extend with decreasing intensity over the full width of the detector. A  $4k \times 4k$  CCD with a pixel size of  $15 \mu\text{m}$  will be a suitable detector to cover the required spectral orders with interleaved spectra without any vignetting. The CCD with low thermal and readout noise along with a high quantum efficiency over the specified wavelength range will be used for this purpose. The detector will be chosen to have more than 60% efficiency in extreme wavelengths.

The efficiency of the instrument will depend upon the efficiency of the individual components used in the instrument and the loss of the light while entering in the slit. Fig. 4 shows the efficiency of both the spectrograph and the telescope + spectrograph. While calculating the efficiency of the spectrograph only, we have taken into account all the components of the spectrograph unit, the telescope interface unit, the detector, and the typical seeing loss for the  $1.1''$  of the sky (e.g. Raskin 2011). The maximum efficiency of the instrument is found in between  $500 - 550 \text{ nm}$ .

The SNR for the proposed spectrograph at  $550 \text{ nm}$  for the DOT was also calculated at the detector adopting total a throughput of 20% for the spectral resolutions of 80 000 and 40 000 at exposure times of 5, 30, and 60 minutes. Figs. 5 and 6 show the SNR for a range of visual magnitudes for the spectral resolution of 80 000 and 40 000, respectively. A SNR of  $\sim 100$  can be achieved for a  $14^{\text{th}}$  magnitude star if a spectral resolution of 80 000 is adopted for 60 min of integration time. Hence, the required SNR can be achieved for the proposed science goals.

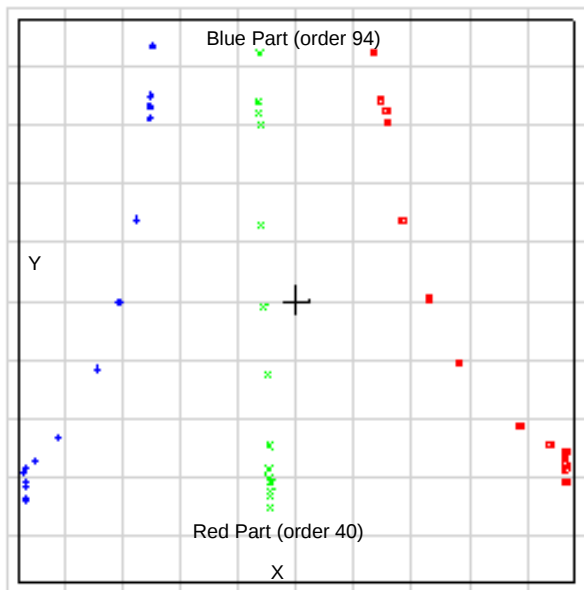


Figure 3: Shape of the spectrum at the CCD plane. The location of the start, center, and end of a few orders are given with blue, green, and red symbols, respectively.

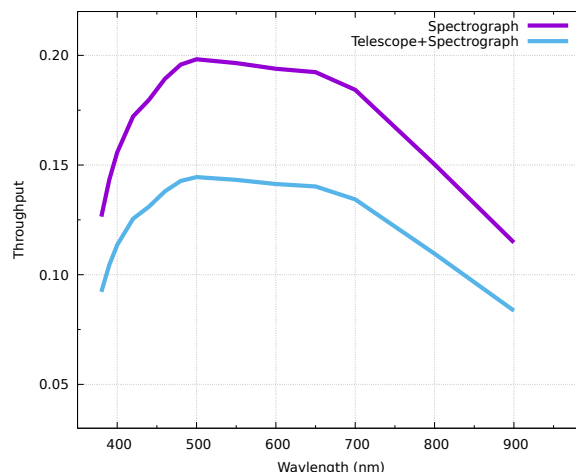


Figure 4: The total throughput of the spectrograph (purple line) and the telescope + spectrograph (blue line). The efficiency of the spectrograph includes all the components from the interface unit, spectrograph unit, detector, and light losses from the slit.

## 5 National and international status of the design

Like many present-day high-resolution spectrographs, the optical layout of the proposed spectrograph is based on a white pupil design, discussed in detail by Baranne (1988). This concept was implemented for one of the first times for the Ultraviolet and Visual Echelle Spectrograph (UVES). It is arguably one of the best solutions for a high-resolution echelle spectrograph. It was also used for other successful ESO spectrographs like the Fibre-fed Extended Range Optical Spectrograph (FEROS) and the High Accuracy Radial velocity Planet Searcher (HARPS). This white pupil design has been adopted in many spectrographs over worldwide. The proposed spectrograph for the DOT will have similar specifications to many other existing high-resolution spectrographs in the world. A few of the modern high-resolution spectrographs are described below for comparison.

UVES is the high-resolution optical spectrograph located at the Nasmyth B focus of the Very Large Telescope (VLT). It is a cross-dispersed echelle spectrograph designed to operate with high efficiency from the atmospheric cut-off at 300 nm to the long wavelength limit of CCD detectors (about 1100 nm). To this aim, the light beam from the telescope is split into two arms (ultraviolet to blue and visual to red) within the instrument. The two arms can be operated separately or in parallel via a dichroic beam splitter. The maximum resolution is 80 000 and 110 000 for the blue- and the red arm, respectively (Dekker et al. 2000). HARPS is a fibre-fed cross-dispersed echelle spectrograph mounted on the 3.6-m telescope in La Silla. Its science driver is the search for extra-solar planets using the radial velocity method with an accuracy of  $1 \text{ m s}^{-1}$  (Mayor et al. 2003). HARPS is designed as an echelle spectrograph fed by a pair of fibres and optimised for mechanical stability. In order to avoid spectral drift due to temperature and air pressure variations, it is placed in a vacuum vessel. The two HARPS fibres (object + sky/Th-Ar) have an aperture on the sky of  $1''$  and deliver a resolving power of 115 000. HARPS produces a SNR of 110 per pixel at 550 nm for a  $6^{th}$  magnitude star in 1 minute integration time. The Echelle SpectroPolarimetric Device for the Observation of Stars (ESPADONS) is also a bench-mounted high-resolution echelle spectrograph and spectropolarimeter. It was designed to

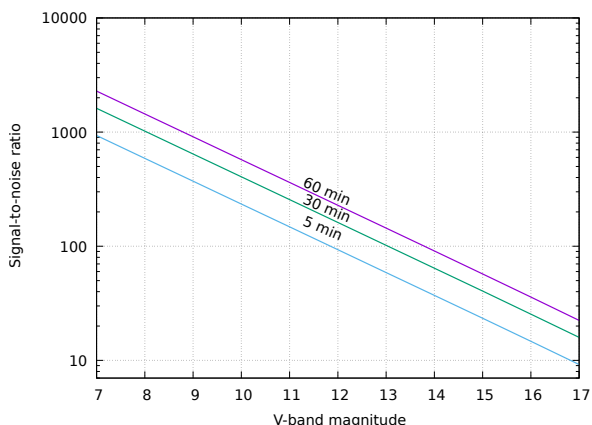


Figure 5: SNR per spectral resolution bin at 550 nm as a function of visual magnitude for 80 000 spectral resolution for three different exposures.

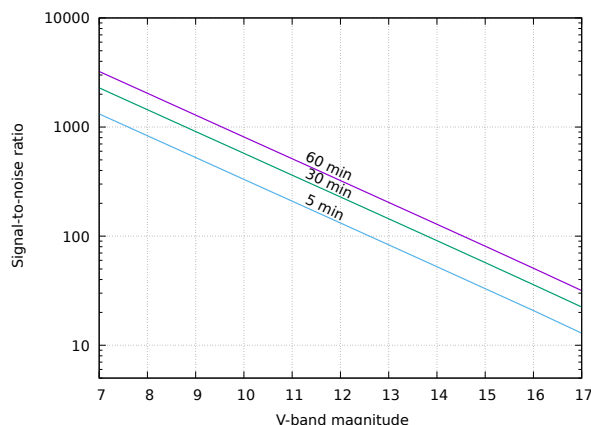


Figure 6: SNR per spectral resolution bin at 550 nm as a function of visual magnitude for 40 000 spectral resolution for three different exposures.

obtain a complete optical spectrum (from 370 to 1050 nm) in a single exposure with a resolving power of about 68 000 and 81 000 in spectropolarimetric and spectroscopic mode, respectively (Donati et al. 2006). ESPADONS is installed on the 3.6-m Canada-France Hawaii Telescope. The High Efficiency and Resolution Mercator Echelle Spectrograph (HERMES) is fibre-fed through an atmospheric dispersion corrector. It is mounted on the Nasmyth A focal station of the 1.2-m Mercator telescope at La Palma. HERMES features a fixed wavelength setting of 377 – 900 nm in a single exposure, with a choice of two observing modes of 85 000 and 62 000 (Raskin et al. 2011). The HRS at the 9-m Hobby-Eberly Telescope (HET; McDonald Observatory, Texas, USA; Tull 1998), the high-resolution spectrograph for the Southern African Large Telescope (SALT; Sutherland, South Africa; Crause et al. 2014), and the TOU spectrograph at the 2-m Automatic Spectroscopy Telescope (AST; Fairborn observatory, Arizona, USA; Ge et al. 2016) are other examples of spectrographs using the white pupil concept.

Within India, two fibre fed white pupil concept based spectrographs are working currently. One is mounted on the 2.0-m Himalayan Chandra Telescope (HCT) of the Indian Institute of Astrophysics (IIA; Bengaluru, India) and the other is mounted on the 1.2-m Mt. Abu telescope of the Physical Research Laboratory (PRL; Ahmedabad, India). The Hanle Echelle Spectrograph (HESP; Sriram et al. 2018) is recently built and mounted on the HCT. This is also a bench mounted fibre-fed spectrograph with two modes of the spectral resolution (30, 000 and 60, 000). It has a compact size, large wavelength coverage of 350 – 900 nm, and a high throughput. The primary aim of the PRL Advanced Radial velocity Abu Sky Search (PARAS; Chakraborty et al. 2010) is to search for planets around a sample of hundreds of cool dwarf main-sequence stars within a volume of 100 pc using the simultaneous Th-Ar calibration technique with the aim to reach a radial velocity precision of  $< 1 \text{ m s}^{-1}$  on bright targets (Chakraborty et al. 2010). The PARAS spectrograph has a spectral resolution of  $\sim 63\,000$  and a wavelength coverage of 370 – 860 nm in the star+calibration mode. Another fibre-fed echelle spectrometer is mounted on the 2.3-m Vainu Bappu Telescope at the Vainu Bappu Observatory (VBO; Kavalur, India) of the IIA. It is based upon the design of the Sandiford Echelle Spectrometer of the 2.1-m telescope of the McDonald Observatory (McCarthy et al. 1993). A spectral resolution between  $\sim 30\,000 - 100\,000$  can be achieved by changing the width of the slit. This spectrograph has a spectral range of 400 – 1000 nm (Rao et al. 2005).

## 6 Summary

A high-resolution spectrograph is planned to be built to carry out a variety of science objectives. The spectrograph design will be based on the white pupil concept which is widely used in modern spectrographs. The proposed scientific objectives require two modes of spectral resolution (around 40 000 and 80 000) over a wavelength range of 380 – 900 nm. It will be designed to have a peak efficiency of  $\sim 18 - 20\%$ . The preliminary design of the spectrograph shows that it will be possible to obtain a spectrum with a spectral resolution of 80 000 and a SNR of 100 for a 14<sup>th</sup> mag with an integration of 60 minutes. It allows to observe the object and an arc/sky spectrum simultaneously.

## Acknowledgments

Acknowledgments go to various people who have given their time to shape the project. Valuable inputs in defining the science goals of the instrument provided by Drs. B. Kumar, R. K. S. Yadav, G. Maheswar, S. B. Pandey, H. Chand, S. Joshi, K. Misra, and Saurabh Sharma are thankfully acknowledged. Past and present directors of ARIES, i.e. Prof. Ram Sagar, Dr. A. K. Pandey, and Dr. Wahab Uddin, are highly acknowledged for their guidance and direction. Guidance from Prof. P. C. Agrawal is highly acknowledged. A team comprising of Prof. S. K. Ghosh, Prof. D. K. Ojha, Prof. R. Srianad, Prof. T. Sivarani, Prof. Abhijit Chakravarti, Prof. N. Kobayashi, and Dr. D. E. Mkrtichian is gratefully acknowledged for defining the technical specifications of the spectrograph. Thanks to Prof. Alain Jorissen, Dr. Peter De Cat, and Dr. Patricia Lampens for their help. Help from Dr. Gert Raskin in starting the optical design of the spectrograph is highly acknowledged. The work presented in these proceedings is supported by the Belgo-Indian Network for Astronomy & Astrophysics (BINA), approved by the International Division, Department of Science and Technology (DST, Govt. of India; DST/INT/Belg/P-02) and the Belgian Federal Science Policy Office (BELSPO, Govt. of Belgium; BL/11/IN07). We thank the referee of this paper for his/her useful comments and suggestions.

## References

- André P., Motte F., Bacmann A. 1999, *ApJ*, 513, 57  
Asplund M., Lambert D. L., Nissen P. E. 2006, *ApJ*, 644, 229  
Baranne P. 1988, in *ESO Conference on Very Large Telescopes and their Instrumentation*, 2, 1195  
Baug T., Ojha D. K., Ghosh S. K. et al. 2018, *JAI*, 750003  
Chakraborty A., Mahadevan S., Roy A. et al. 2010, *SPIE*, 7735, 4  
Charbonnel C., Primas F. 2005, *A&A*, 442, 961  
Collier-Cameron A. 2001, *LNP*, 573, 183  
Croswell K., Hartmann L., Avrett E. H. 1987, *ApJ*, 312, 227  
Crause L. A., Sharples R. M., Bramall D. G. et al. 2014, *SPIE*, 9147, 6  
Dekker H., D’Odorico S., Kaufer A., Delabre B., Kotzlowski H. 2000, *SPIE*, 4008, 534  
D’Ercole A., D’Antona F., Ventura P. et al. 2010, *MNRAS*, 407, 854  
De Mauro M. P. 2016, *PoS*, 29  
Donati J. F., Catala C., Landstreet J. D., Petit P. 2006, *ASPC*, 358, 362  
Dunham M. M., Evans N. J., Bourke T. L. 2010, *ApJ*, 721, 995  
Durgapal A. K., Pandey A. K. 2001, *A&A*, 375, 840, 2001  
Ge J., Ma B., Sithajan S. et al. 2016, *SPIE*, 9908, 6  
Gratton R. G., Carretta E., Bragaglia A. 2012, *A&ARv*, 20, 50  
Hartmann L., Kenyon S. J. 1996, *ARA&A*, 34, 207  
Joshi A., Pandey J. C., Singh K. P., Agrawal P. C. 2016, *ApJ*, 830, 56  
Joshi A., Pandey J. C. 2018, *BSRSL*, 87, 176  
Joshi R., Chand H., Gupta A. C., Wiita P. J. 2011, *MNRAS*, 412, 2717

- Joshi S., Mary D. L., Martinez P. et al. 2006, *A&A*, 455, 303  
Joshi S., Joshi Y. C. 2015, *JApA*, 36, 33  
Joshi Y. C., Pandey A. K., Narasimha D., Sagar R. 2005, *A&A*, 433, 787  
Kopatskaya E. N., Kolotilov E. A., Arkharov A. A. 2013, *MNRAS*, 434, 38  
Kumar B., Omar A., Gopinathan M. et al. 2018, *BSRSL*, 87, 80  
Kurucz R. L. 2014, in *Determination of Atmospheric Parameters of B-, A-, F- and G-Type Stars*, 25, Springer International Publishing, Editors: Ewa Niemczura, Barry Smalley and Wojtek Pych, 25  
Lata S., Pandey A. K., Panwar N. et al. 2016, *MNRAS*, 456, 2505  
Lata S., Pandey A. K., Pandey J. C. et al. 2019, *AJ*, 158, 51  
Lee J.-E., Di Francesco J., Bourke T. L. et al. 2007, *ApJ*, 671, 1748  
Mayor M., Pepe F., Queloz D. et al. 2003, *Msngr*, 114, 20  
Mayor M., Queloz D. 1995, *Nature*, 378, 355  
McCarthy J. K., Sandiford B. A., Boyd D., Booth J. 1993, *PASP*, 105, 881  
Medhi B. J., Maheswar G., Brijesh K. et al. 2007, *MNRAS*, 378, 881  
Misra K., Sahu D. K., Anupama G. C. 2008, *MNRAS*, 389, 706  
Mohan V., Uddin W., Sagar R., Gupta S. K. 1999, *BASI*, 27, 601  
Ojha D., Ghosh S. K., Sharma S. et al. 2018, *BSRSL*, 87, 580  
Omar A., Kumar B., Gopinathan M., Sagar R. 2017, *CSci*, 113, 682  
Omar A., Kumar T. S., Krishna R. B., Pant J., Mahto M. 2019a, *CSci*, 116, 1472  
Omar A., Saxena A., Chand K. et al. 2019b, *JApA*, 40, 9  
Pandey A. K., Mahra H. S. 1986, *Ap&SS*, 120, 107  
Pandey J. C., Medhi B. J., Sagar R., Pandey A. K. 2009, *MNRAS*, 396, 1004  
Pandey J. C., Singh K. P., Drake S. A., Sagar R. 2005, *AJ*, 130, 1231  
Pandey S. B., Anupama G. C., Sagar R. et al. 2003a, *MNRAS*, 340, 375  
Pandey S. B., Sahu D. K., Resmi L. et al. 2003b, *BASI*, 31, 19  
Pandey S. B., Yadav R. K. S., Nanjappa N. et al. 2018, *BSRSL*, 87, 42  
Pandey S. B., Hu Y., Castro-Tirado A. J. et al. 2019, *MNRAS*, 485, 5294  
Patel M. K., Pandey J. C., Karmakar S., Srivastava D. C., Savannov I. S. 2016, *MNRAS*, 457, 3178  
Rao N. K., Sriram S., Jayakumar K. et al. 2005, *JApA*, 26, 331  
Raskin G. 2011, PhD thesis, KU Leuven  
Raskin G., Van Winckel H., Hensberge H. et al. 2011, *A&A*, 526, 69  
Reipurth B., Aspin C. 2010, in *Evolution of Cosmic Objects through their Physical Activity*, Proceedings of the Conference dedicated to Viktor Ambartsumian's 100th anniversary, 19  
Ricker G. R., Winn J. N., Vanderspek R. et al. 2014, *SPIE*, 9143, 20  
Rice J. B. 2002, *AN*, 323, 220  
Sagar R., Joshi U. C. 1983, *MNRAS*, 205, 747  
Sagar R., Krishna G., Mohan V. et al. 1999, *A&AS*, 134, 453  
Sagar R., Uddin W., Pandey A. K. et al. 2000, *A&AS*, 114, 349  
Sagar R., Kumar B., Omar A., Pandey A. K. 2012, *SPIE*, 8444E, 1TS  
Sing D. K., Fortney J. J., Nikolov N. et al. 2016, *Nature*, 529, 59  
Singh M., Misra K., Sahu D. K. et al. 2018, *MNRAS*, 474, 2551  
Shu F. H., Adams F. C., Lizano S. 1987, *ARA&A*, 25, 23  
Sriram S., Kumar A., Surya A. et al. 2018, *SPIE*, 10702, 6  
Strassmeier K. G., Rice J. B. 2003, *A&A*, 399, 315  
Tull R. G. 1998, *SPIE*, 3355, 387  
Vogt S. S., Penrod G. D. 1983, *PASP*, 95, 565  
Young C. H., Jorgensen J. K., Shirley Y. L. 2004, *ApJS*, 154, 396